Published in final edited form as:
Nat Neurosci. 2012 September ; 15(9): 1265–1271. doi:10.1038/nn.3176.

Behavior-dependent specialization of identified hippocampal interneurons

Damien Lapray[1,2], **Balint Lasztoczi**[1,2], **Michael Lagler**[2], **Tim James Viney**[1], **Linda Katona**[1], **Ornella Valenti**[2], **Katja Hartwich**[1], **Zsolt Borhegyi**[2], **Peter Somogyi**[1,2], and **Thomas Klausberger**[1,2]

[1]MRC Anatomical Neuropharmacology Unit, Department of Pharmacology, Oxford University, UK

[2]Center for Brain Research, Dept. Cognitive Neurobiology, Med. Uni. Vienna, Austria

Abstract

A large variety of GABAergic interneurons control information processing in hippocampal circuits governing the formation of neuronal representations. Whether distinct hippocampal interneuron types contribute differentially to information-processing during behavior is not known. We employed a novel technique for recording and labeling interneurons and pyramidal cells in drug-free, freely-moving rats. Recorded parvalbumin-expressing basket interneurons innervate somata and proximal pyramidal cell dendrites, whereas nitric-oxide-synthase- and neuropeptide-Y-expressing ivy cells provide synaptic and extrasynaptic dendritic modulation. Basket and ivy cells showed distinct spike timing dynamics, firing at different rates and times during theta and ripple oscillations. Basket but not ivy cells changed their firing rates during movement, sleep and quiet wakefulness, suggesting that basket cells coordinate cell assemblies in a behavioral state-contingent manner, whereas persistently-firing ivy cells might control network excitability and homeostasis. Different interneuron types provide GABA to specific subcellular domains at defined times and rates, thus differentially controlling network activity during behavior.

GABAergic interneurons control information processing in cortical circuits as percussionists set the rhythm for a melody, or traffic lights regulate the movement of cars through a city. Interneurons generate oscillatory activity[1, 2], synchronize the activity of pyramidal cells[3] and set time windows for synaptic integration[4]. A large diversity of interneuronal types is a hallmark of cortical circuits. Different domains of pyramidal cells, such as the soma, axon-initial-segment, proximal or distal dendrites[5] are innervated by distinct types of GABAergic interneuron. They also have distinct inputs and membrane properties[6-10] and show different firing patterns during network oscillations induced in vitro[11-14] or recorded in anesthetized animals[15], indicating distinct roles for specific interneuron types. However, research on interneurons in drug-free animals that can freely change their behavior, has so far been limited to recordings from unidentified interneurons because of technical limitations. In the barrel cortex of head-restrained mice, groups of interneurons with distinct membrane dynamics during different behavioral states have been described[16, 17] and in the hippocampus unidentified interneurons or interneurons belonging to heterogeneous groups expressing parvalbumin and/or somatostatin have been reported[18-21] to fire with different firing patterns during network oscillations. But, how do specific types of identified interneurons control the activity of cortical circuits in freely-moving animals? Could

Correspondence and requests for materials should be addressed to D.L. (damien.lapray@pharm.ox.ac.uk) or P.S. (peter.somogyi@pharm.ox.ac.uk) or T.K. (thomas.klausberger@meduniwien.ac.at).

Author contributions: All authors contributed to experiments, analysis and manuscript preparation.

Europe PMC Funders Author Manuscripts

different types of interneuron make distinct contributions to the information processing during different behaviors? To address these questions we developed a novel technique that allows recordings from unequivocally-identified neurons in naturally behaving animals and discovered how two most prominent types of hippocampal interneuron contribute to different behavioral states and network operations.

Results

Identification of neurons recorded in freely-moving rats

We recorded the activity of parvalbumin (PV)-expressing basket, ivy and pyramidal cells in the dorsal CA1 area with glass electrodes while drug-free rats were behaving in a recording arena without restraint during movement, natural sleep and quiet wakefulness. Subsequently, recorded cells were juxtacellularly labeled[22] for cell type identification. We used novel microdrives for glass electrode placement (Narishige, Kleindiek), mini-preamplifiers (NPI Electronic) as well as a stable or moveable[23] metal reference electrode in CA1 of the hippocampus or neocortex. A screw in the skull for EEG recordings and tracking devices enabled monitoring of neuronal and behavioral activity. A detailed description on the method is reported in the supporting online material.

Parvalbumin-expressing basket cells[5] (n=5) were identified based on their immunoreactivity for PV and their axonal branching in the stratum-pyramidale and adjacent layers, where they innervate somata and proximal dendrites of pyramidal and other neurons (Fig 1). For one cell (TV08k) we performed an electron microscopic analysis of 11 randomly sampled synapses and found as synaptic targets: the somata (45%), somatic spines (18%) or dendrites (27%) of pyramidal cells, as well as interneuron dendrites (9%). All basket cells reported here expressed the Ca^{2+}-binding protein parvalbumin and the ErbB4 receptor[24] (Fig. 1 and Table 1; primary antibodies are listed in Supplementary Table 1). Ivy cells[25, 26] (n=3) had very fine and dense axons in the stratum-radiatum and stratum-oriens providing synaptic and extrasynaptic GABAergic input to pyramidal cell dendrites. Two out of three cells[27] were immunopositive for neuronal nitric oxide synthase (nNOS), and all tested cells expressed neuropeptide tyrosine (NPY) and a high level of neurokinin 1 receptor (NK1R), as well as the α1 and δ subunits of $GABA_A$ receptors in the somato-dendritic membrane (Fig. 2 and Table 1). We also analyzed recordings of 14 CA1 pyramidal cells (n=4 labeled) during different behaviors. Some of these neurons fired as place cells[28-30] during spatial navigation and we tested some of their molecular expression patterns (Fig. 3 and Table 1).

Behavior-specific firing of distinct neurons

For the definition of behavioral states (Fig. 4 and **online methods**) we used several parameters including tracking of movements with LED-video-monitoring and/or an accelerometer. We also used the occurrence of characteristic events such as spindles in the EEG. Pyramidal cells fired with similar mean rates during body-movement, slow-wave-sleep and quiet wakefulness at 2.6±2.3, 1.7±1.4, and 2.2±1.8 Hz (mean±SD), respectively ($p=0.6$ for paired Friedman test; $p=0.3$ for repeated measures ANOVA; n=12). However, they showed large variability for different cells and also between different periods for the same cell. In contrast, PV-expressing basket cells appeared to change their firing rate dynamically according to the ongoing brain state (Fig. 5a). To quantify this observation we tested individual basket cells and found that four out of four tested cells fired at different rates during body-movement, slow-wave-sleep and quiet wakefulness ($p<0.05$, Kruskal Wallis test; the fifth basket cell was not included for this analysis because only one episode of slow-wave-sleep was recorded). Quite the opposite, none of the three ivy cells showed such behavioral state-dependent differences ($p>0.1$) in firing activity (Fig. 5b). As a group (Fig. 5c), the mean firing rates of PV-expressing basket cells (n=5) differed ($p=0.009$ for

paired Friedman test; p=0.004 for repeated measures ANOVA) during slow-wave-sleep (31±10 Hz), quiet wakefulness (17±7 Hz) and body-movement (24±11 Hz). A post-hoc Dunn or Bonferronís test indicated a difference (p<0.05) between firing during slow-wave-sleep and quiet wakefulness. In contrast, ivy cells discharged with similar mean rates (p=0.9 for paired Friedman test; p=0.9 for repeated measures ANOVA; n=3) at 4.0±1.3, 3.8±0.6, 3.8±1.8 Hz during body-movement, slow-wave-sleep and quiet wakefulness, respectively. A mixed-model two-way ANOVA analysis indicated a significant interaction (p=0.03) between the factor cell type and the repeated-measure factor behavioral state (p<0.001 for subject matching shows that the repeated-measures design was effective in controlling for the observed variability, Fig. 5c). This suggests that the firing rate changes of the two cell types during distinct behavioral states were different.

Furthermore, we investigated the changes in the interspike intervals of PV-expressing basket and ivy cells during different behavioral states (Fig. 5d). Overall, PV-expressing basket cells fired with shorter interspike-intervals compared to ivy cells. In addition, PV-expressing basket cells had a higher proportion of interspike-intervals at beta and gamma frequency during movement in comparison to slow-wave-sleep and quiet wakefulness, but interspike intervals at beta or gamma frequency were hardly observed for ivy cells during movement. This demonstrates that these two types of GABA-releasing interneuron contribute differentially to the organization of the hippocampal network during distinct behavioral states.

Network oscillation-specific firing of distinct neurons

We also measured behavior-dependent network oscillations in the local field potential (LFP) recorded extracellularly in the stratum-pyramidale with a metal reference or the glass electrode. Theta oscillations (5-12 Hz) were detected during body-movements, paradoxical sleep and occasionally during quiet wakefulness. Sharp wave associated ripples (130-230 Hz) were detected during slow-wave-sleep and quiet wakefulness. Notably, we also observed short periods with overall low oscillatory activity (Fig. 6b). These periods often occurred at transitions between different behavioral states. We defined these periods of overall low oscillatory activity when the power in the theta, beta, slow and fast gamma bands simultaneously dropped below a set threshold (mean – SD of the root mean square amplitude in the respective frequency band). After defining the periods of different network oscillations, we analyzed the firing rates of distinct neurons. Pyramidal cells fired with 2.6±2.6, 6.5±5.4, and 0.8±0.9 Hz during theta oscillations, ripples, and low oscillatory periods, respectively (p=0.0001 for paired Friedman test and p<0.05 for post-hoc Dunn test for ripples versus theta oscillations and ripples versus low oscillatory periods; p=0.0007 for repeated-measure ANOVA and p>0.05 for post-hoc Bonferronís test for ripples versus theta oscillations and ripples versus low oscillatory periods; n=14). Parvalbumin-expressing basket cells fired differently (Fig. 6a; p=0.008 for paired Friedman test; p<0.0001 for repeated-measure ANOVA; n=5) during theta oscillations (21±5 Hz), ripples (122±32 Hz) and low oscillatory periods (6.5±3.4 Hz) (p<0.05 for firing during ripples versus low oscillatory periods with post-hoc Dunn test; p<0.05 for firing during ripples versus low oscillatory periods and firing during theta oscillations versus low oscillatory periods for repeated-measure ANOVA). In contrast, ivy cells fired with similar rates during the three oscillatory states (p=0.4 for paired Friedman test; p=0.6 for repeated-measure ANOVA; n=3; 2.8±0.8, 5.2±6.9, 2.1±1.0 Hz during theta, ripple oscillations and low oscillatory periods, respectively).

Next, we investigated whether PV-expressing basket and ivy cells exhibit different firing patterns during the network oscillations. We observed that PV-expressing basket cells follow the high frequency ripple oscillations with strong discharges (Fig. 6c) in contrast to ivy cells (Fig. 6d) which often remained silent during ripples. Individual PV-expressing

basket cells fired with 4 to 11 (median) spikes per sharp wave-associated ripple episode. In contrast (p=0.03, Mann Whitney test), individual ivy cells showed zero or 1 spike (median) per sharp wave-associated ripple episode (Fig. 6e). Notably, ivy cell M66a, which fired with a median of 1 spike per ripple episode, was nNOS-immunonegative and had higher immunoreactivity for δ subunits of $GABA_A$ receptors in the somato-dendritic membrane (Table 1). Such highly δ subunit-immunoreactive ivy cells are a minority of the overall population (their Suppl. Fig. 6 in [31]).

During theta oscillations we observed different spike timing of PV-expressing basket and ivy cells. The phase of theta oscillations was always detected in the pyramidal cell layer with either the glass or a metal reference electrode. Basket cells fired at the descending phase of field theta oscillations, on average at 289° ± 48° (0° and 360° mark the trough). In contrast ivy cells fired at the trough and ascending phase of field theta oscillations, on average at 46° ± 37°. There was no overlap in the mean firing phase of individual basket and ivy cells (Fig. 6g), indicating that the two cell types modulate pyramidal place cells at different times of the theta cycle. Notably, individual basket cells showed some variability in their mean firing phase during theta oscillations (Fig. 6g). The mean firing phase of individual basket cells was similar during theta oscillations occurring at different behavioral states, suggesting that different brain states were not responsible for this variability. However, a relation between the mean firing phase during theta oscillations and the position of the cell within the hippocampus (Supplementary Fig. 1) was observed. For this analysis the theta phase was always detected locally from the glass electrode. We observed that PV-expressing basket cells with positions more posterior and lateral within the dorsal CA1 area fired at later phases of the local field theta oscillations (Fig. 6f). This observation might reflect a traveling wave of theta oscillations across the hippocampus[32, 33].

Ivy cells fired with similar firing rate across different behavioral states and network oscillations. However, during theta oscillations we observed some fluctuations in firing rate within the same period (Fig. 7a). These fluctuations seemed to be related to the frequency and amplitude of the field theta oscillations. For two ivy and two basket cells sufficient theta oscillations at different frequencies and amplitudes were recorded to analyze this observation in detail (Fig. 7b). The LFP recordings during theta oscillations were subjected to a continuous Morlet wavelet transformation and the instantaneous amplitudes were Z-transformed for each frequency line independently. Amplitude/frequency spectrum averages were plotted against the instantaneous firing rate of the recorded cells in a 200 ms window (**see online methods**). Ivy cells fired sparsely during theta oscillations, hence in any 200 ms window there were only a few or no spikes (the x-axis spans a range only between 0 and 4 spikes per 200 ms). Nevertheless, the firing rate of both ivy cells showed a clear relationship with the frequency and the amplitude of the theta oscillations, i.e. an acceleration of theta together with an increase in the cells' firing (Fig. 7b). The firing rate of PV-expressing basket cells varied across a much wider dynamic range, but the frequencies of LFP amplitude maxima show only minor acceleration with increasing spike rate for most of the dynamic range. Although in general the firing rate of the PV-expressing basket cells increased together with the amplitude of theta oscillations, for most of the dynamic range an increase in the LFP frequency was not associated with increased firing rates. In summary, both cell types increased their firing with increasing theta amplitude in the LFP. In addition, ivy cells also increased their firing rate with faster frequency theta oscillations (Fig. 7b).

Discussion

Our results show that two distinct types of GABAergic interneuron, PV-expressing basket and ivy cells, the two most numerous GABAergic cell types in the hippocampal pyramidal layer, contribute differentially to behavioral state-dependent neuronal activities and

oscillatory network operations in freely-moving rats. Parvalbumin-expressing basket cells are the most studied type of cortical interneuron. So far, an unequivocal recognition of PV-expressing basket cells is only possible by verifying both their molecular expression and axonal arborizations, because PV is expressed also by hippocampal axo-axonic, bistratifed, O-LM and some long-range projection neurons and because other types of basket cell exist which do not express parvalbumin[34]. Parvalbumin-expressing basket cells are thought to contribute to the generation of network oscillations[2, 13, 15, 35, 36] through their highly precise inhibitory control of pyramidal cell output[5, 37-39]. They have been predicted to provide a clock-like temporal frame for information coding by pyramidal cells[40]. However, our results show that, in addition, the output of PV-expressing basket cells is dynamically adjusted strongly depending on the ongoing behavior. They are most active during slow-wave-sleep, when sequences of cell assemblies are frequently replayed during sharp wave-associated ripples, which contribute to memory consolidation and transfer to the neocortex[41, 42]. Basket cells also provide rhythmic GABAergic input during body-movement, they fire at the descending phase of theta oscillations, when pyramidal place cells stop phase-precessing firing and are least active. Notably, we have found that when the animal pauses at behavioral state transitions, oscillatory activity can drop in several frequency bands accompanied by a decrease in the firing of PV-basket cells. This reduced temporal structure may allow network reorganization and the emergence of new cell assemblies.

In contrast to PV-expressing basket cells, which dynamically change their activity during different behaviors, ivy cells fire on average with similar rates during slow-wave-sleep, body-movement, quiet wakefulness, and different network oscillations. Ivy cells are the quantitatively most abundant type of GABAergic interneuron in the CA1 area[25]. They provide widespread synaptic and extrasynaptic slow GABAergic input, as well as NPY and nitric oxide to pyramidal cell dendrites and Schaffer collateral/commissural terminals via their exceptionally dense axonal arborizations[25, 26] and may mediate the activity-dependent regulation of neurogenesis[43]. The firing patterns identified here, are well suited to control homeostasis in the network. We observed that pyramidal cells fire, on average, with similar rates during different behavioral states and they are under constant control via the volume transmission[44] by GABA, NPY and nitric oxide from the dense axonal web of ivy cells. In addition, we observed that ivy cells fire with higher rates when field theta oscillations become faster in frequency and larger in amplitude reflecting increased network activity and synchrony.

Notably, PV-expressing basket or ivy cells reported here have similar spike timing relative to theta oscillations compared to those recorded under anesthesia[15, 25]. This is remarkable considering that the frequency of theta oscillations is twice as high in drug-free compared to anesthetized preparations, and the average firing rates of the neurons are higher in the absence of anesthesia. The preservation of firing phase and the presumed lack of pyramidal cell firing as place or grid cells in the anesthetized rat, suggest that the spike timing of interneurons during theta oscillations might be controlled also by external inputs including those from the medial septum. Furthermore, the firing patterns of each cell type during sharp wave-associated ripples also resembled those recorded under anesthesia. Parvalbumin-expressing basket cells strongly increased firing, whereas ivy cells did not change their firing rate. Such a preservation of cell type-specific network contribution suggests robust internal network controls across a wide range of input strengths.

Overall, our results show differential contributions of distinct types of interneuron to different behaviors and network operations in freely-moving rats, explaining why the temporal dynamics of GABA release is supported by independent sources from specific interneuron types. Because different types of interneuron also provide GABA to different

subcellular places, a spatio-temporal matrix of GABAergic inputs dynamically regulates neuronal computations during different behavioral activities.

Online Methods

Subjects and housing conditions

All procedures involving animals were performed according to methods approved by the UK Home Office and The Animals (Scientific Procedures) Act (1986) and were approved by the Institutional Animal Care and Use Committee of the University of Oxford and of the Medical University Vienna. Twenty Sprague-Dawley rats (300-550 g) were used in this study. Upon arrival, animals were housed in groups of 2-4 per cage in Oxford (16 rats; 19-21C°; 55% humidity; reverse light/dark cycle, lights on from 20:00 to 8:00) or Vienna (4 rats; diurnal cycle, lights on from 6:00 to 18:00). One to 7 days before the protocol started, rats were housed individually with *ad libitum* access to food pellets and water. In addition, chocolate chips were provided to habituate 3 of the rats to a reward provided during some experimental recordings.

Headstage implantation

Rats were anesthetized with isoflurane (IsoFlo, Abbott) with supplemental i.p. administration of Fentanyl-Janssen® (4 μl/100g; Janssen-Cilag, Vienna) in 3 rats, and mounted in a stereotaxic frame (Kopf Instruments). Body temperature was maintained at 37 ± 0.5 °C with a heating pad and breathing was monitored. The skull was exposed and cleaned. Five stainless steel screws were attached to the bone. One was placed above the right prefrontal cortex for EEG recordings (4/2 mm anterior/lateral from bregma); another screw above the cerebellum served as as ground/reference. A cylindrical holder for the microdrive was positioned above the left parietal cortex and EEG and ground screws were connected to a main connector placed above the frontal part of the skull. The whole headstage was embedded in dental acrylic (Refobacin bone cement R, Biomet) except for the region overlying the right hippocampus. The edges of the construction were covered with a smooth layer of blue light sensitive cement (Tetric EvoFlow, Ivoclar Vivadent). All rats were given analgesic treatments (subcutaneous injection of 0.05 ml Rimadyl®, Pfizer, or Dipidolor, Janssen-Cilag, 2ml/125ml drinking water provided for 48h after surgery) and some were also given antibiotics (intra-peritoneal injection of 0.1 ml Baytril® 2.5 %, Bayer Vital). Animals were allowed at least 3 recovery days after headstage implantation. Three rats were food restricted to reach ~85% initial weight before recording started.

Craniotomy and duratomy

After the recovery period, animals were anesthetized with isoflurane and mounted in a stereotaxic frame. Craniotomy and duratomy were performed above the right hippocampus. In between these two procedures 0.1 mg/ml of Mitomycin C was applied on the dura mater for 10 min to reduce growth-tissue on subsequent days. A single wire (50 μm tungsten, California Fine Wire) was placed in the hippocampus or cortex and either fixed on the skull or mounted on a miniature drive[23]. The cortical surface was protected by a layer of silicone (Kwik-Sil™, World Precision Instruments).

Juxtacellular recording and labeling in freely moving rats

One to 10 days after duratomy, the animals were anesthetized with isoflurane and mounted in a stereotaxic frame with the ear bars attached directly to the headstage as support. A glass electrode, containing 1.5 or 3 % neurobiotin in 0.5 M NaCl, mounted on a custom-made hydraulic (Narishige) or piezoelectric[45] (Kleindiek Nanotechnik) microdrive, was inserted into the cortex. A miniature pre-amplifier (ELC mini-preamplifier, NPI Electronic) and two

LED arrays were connected. In 6 rats an accelerometer (Supertech International Ltd) detected head movements. The cortical surface was protected with wax and the animals were placed in the recording arena (length/width/height Oxford: 50/50/30 cm; Vienna: 40/60/30 cm). Animals recovered within 5-10 min from anesthesia as reported previously[46], but recording from hippocampal neurons started more than one hour after recovery from anesthesia (109.4 ± 55.1 min; only two pyramidal cells were recorded before one hour, after 25 and 50 min respectively, neither was labeled). Recordings occurred during day time in a room with partially obscured windows (Vienna) or in a darkened room with ambient light (Oxford, mesopic conditions). None of the rats were exposed to the arena before the first recording. After recording, the electrode was advanced towards the recorded neuron for juxtacellular labeling with neurobiotin[22]. Cells were recorded on days 1 to 12 after duratomy (average 4.6 ± 4.28 days). At the end of the session, the animal was remounted in the stereotaxic frame under isoflurane anesthesia. Recording devices were removed. After successful juxtacellular labeling, the animal was anesthetized and perfusion fixed (see below). If no cell was labeled, the cortex was covered with silicone, the animal was put in its home cage and the procedure was repeated on following days.

Data acquisition

Signals were amplified 1000x (BF-48DGX and DPA-2FS signal conditioners, NPI Electronic) and digitized at 20 kHz (Power1401 A/D board, Cambridge Electronic Design). Wide-band signals (0.3 Hz-10 kHz) were acquired in parallel with online filtered single-units (0.8-5 kHz) and LFP (0.3-500 Hz) components from the glass electrode. Signals from the hippocampal/cortical electrode and the EEG screw were filtered online at 0.3 Hz-10 kHz. Hum-bugs (Digitimer) were used to remove 50 Hz noise without phase-shift. Data from the accelerometer were captured at 1 or 20 kHz from three axes. Signals and video were acquired using Spike2 software (version 7.01, Cambridge Electronics Design) on a personal computer. LED arrays were tracked using a second video camera (Sony, 25 frames sec^{-1}) and synchronized with the electrophysiological recordings (courtesy of Dr Kevin Allen).

Immunohistochemical analysis

One to 4 h after cell labeling, cardiac perfusion with saline was followed by ~20 min fixation (4 % paraformaldehyde, 15 % v/v saturated picric acid and 0.05 % glutaraldehyde in 0.1 M phosphate buffer at pH ~7.2). Tissue preparation and analysis for light, immunofluorescence[47] (primary antibodies are listed in Supplementary Table 1) and electron microscopy[25] was performed as described previously. Two-dimensional reconstructions were made using a drawing tube with a 63x oil-immersion objective.

Analysis of network oscillations

Analysis of network oscillations were performed as described previously[15, 47, 48] with adjustments for different oscillatory frequencies in drug-free rats. Data processing was done with Spike2 or MATLAB (including the Wavelet Toolbox, version 7.9-R2009b; MathWorks). Periods when the glass electrode might have influenced the firing of the cell were excluded.

The detection of sharp-wave/ripple events, the calculation of discharge frequencies were achieved as described previously[47]. The field potential was filtered between 130 and 230 Hz (Spike2 FIR filter) and the RMS power integrated in a 10 ms sliding window. Peaks of at least 5 standard deviations above the mean were considered. All events were validated individually.

The detection of theta epochs were performed as described previously[47]. The theta (5-12 Hz) to delta (2-4 Hz) frequency power ratio was calculated in a 2 s window. A ratio greater than 4 in one window defined a putative theta period. The exact beginning and end points were adjusted manually. Using slightly different detection criteria[49] resulted in the definition of similar theta epochs.

For the detection of low oscillatory periods, the RMS amplitude was calculated in 2 s sliding windows for: 5-15, 15-30, 30-70 and 70-120 Hz. A period was accepted when the RMS was below threshold (mean-1xSD) for all four bands simultaneously and for at least 0.3 s. Boundaries were set when the second frequency band dropped below the threshold (start) and the third frequency band reached the threshold (end).

Recordings of the LFP were down-sampled to 1000 Hz and subjected to a continuous complex-wavelet transformation (Morlet wavelet; wavelet parameters of 1 and 1.5, 38 logarithmically equidistant scales between 5 and 13 Hz). The wavelet transforms were cropped for theta periods (see above), the modulus (instantaneous amplitude) values were extracted and Z-transformed for each scale (frequency line) independently. The amplitude spectra corresponding to individual samples were averaged according to the instantaneous spike rate. Instantaneous rate was binned from 0 to n, with increments of 1, where the cumulative number of samples falling into bins from 0 to n, included at least 99.9 % of all samples (any samples with instantaneous rates above n were added to the bin n).

Definition of behavioral states

Vigilance states were scored manually. Wakefulness was characterized by desynchronized low-amplitude EEG signals lacking spindle oscillations and further segmented into quiet wakefulness (363 episodes, 12.04 s on average ranging from 0.3 to 110 s) and movement (351 episodes, 7.84 s on average ranging from 0.34 to 165 s) depending on movement detection (Fig. 4). Slow-wave-sleep (105 episodes, 38.7 s on average ranging from 6.4 to 269 s) was defined as the state with high-voltage, slow delta waves (< 3 Hz) associated with spindle oscillations (9-14 Hz) and absence of motor activity. Paradoxical sleep (10 episodes, 78.6 s on average ranging from 5 to 250 s) epochs, always occurring after slow-wave-sleep, were defined by a predominant and regular EEG theta rhythm (5-12 Hz) and, despite no movements, the presence of phasic movement twitches. A transition state from slow-wave-sleep to paradoxical sleep was identified when spindles and dominant theta oscillation, on EEG and CA1 LFP respectively, were simultaneously recorded for several seconds.

Statistical analysis

Statistical analysis was performed with GraphPad Prism5, MATLAB and the Circular Statistics Toolbox by Philipp Berens[50]. Comparisons of firing rates were carried out with non-parametric tests, with the exception of the 2-way ANOVA analysis, for which an appropriate non-parametric equivalent is not available. For comparisons of paired data within cell types, in addition to the non-parametric Friedman test, a putatively more powerful repeated-measure ANOVA was also performed and results for both tests are reported.

A mixed-model 2-way ANOVA analysis was only considered if for subject matching $p<0.05$ indicated an effective controlling for data variability (GraphPad Prism5). To further test whether the significant interaction observed for data shown in Fig. 5c was caused only by the different overall firing rates of the two cell types, the average firing rate of the respective cell type was subtracted from all observed firing rate values. The mixed-model 2-way ANOVA analysis on this transformed data resulted in a significant interaction of the factor cell type and the repeated-measure factor behavioral state ($p=0.01$). In another test, all firing

rates of ivy cells were multiplied by 4.75 to achieve a simulated match in baseline firing with PV basket cells (same mean firing rate during quiet wakefulness). Also in this transformed data the mixed-model 2-way ANOVA analysis resulted in a significant interaction of the two factors ($p<0.05$).

We tested the robustness of the observation of similar firing rates of ivy cells (n=3) during different behaviors (Fig. 5) or network oscillations (Fig. 6). First, we checked if the test is powerful enough to detect possible differences with n=3. We repeatedly selected three cells from the five PV-expressing basket cells. Ten out of ten possible data combinations for network oscillations and seven out of ten possible data combinations for behavioral states still showed significant differences for PV-expressing basket cells ($p<0.05$; repeated-measure ANOVA, n=3), indicating that significant changes in firing rate could be observed with n=3. In another test we duplicated the observed data for ivy cells (increase of n with low variance), and their firing rate changes remained non-significant ($p>0.25$, repeated-measure ANOVA, n=6). In a different control test, the observed data were supplemented with two values generated randomly within the mean±SD range of the respective dataset (increase of n with large variance) and again the firing rate changes of ivy cells remained non-significant in all of ten randomly generated datasets ($p>0.12$, repeated-measure ANOVA, n=5). These tests based on simulated data, taken together with tests on individual ivy cells (Fig. 5b) and the 2-way ANOVA analysis (Fig. 5c), support the observation of similar firing rates of ivy cells across different behavioral states.

Supplementary Material

Refer to Web version on PubMed Central for supplementary material.

Acknowledgments

The authors thank Artur Koroknai for the reconstruction of the dendritic tree of cell D26p; Istvan Lukacs for the reconstruction of cell TV08k; Jozsef Somogyi for confocal microscopic data acquisition and illustrations; Kristina Detzner for electron microscopy and immunohistochemistry; Romana Hauer and Erzsebet Borok for histological processing; Tomoya Sakatani for contributions to microdrive development; Ben Micklem for help with the preparation of illustrations; Joseph O'Neill for help with place cell analysis; Yannis Dalezios and Georg Dorffner for advice on statistics; Ray Guillery, David Dupret, Marco Capogna, Jozsef Csicsvari, and Laszlo Marton for comments on an earlier version of the manuscript. This work was supported in part by the ERC, WWTF and FWF.

References

1. Buzsaki, G. Rhythms of the brain. Oxford University Press; New York: 2006.
2. Cardin JA, et al. Driving fast-spiking cells induces gamma rhythm and controls sensory responses. Nature. 2009; 459:663–667. [PubMed: 19396156]
3. Cobb SR, Buhl EH, Halasy K, Paulsen O, Somogyi P. Synchronization of neuronal activity in hippocampus by individual GABAergic interneurons. Nature. 1995; 378:75–78. [PubMed: 7477292]
4. Pouille F, Scanziani M. Enforcement of temporal fidelity in pyramidal cells by somatic feed-forward inhibition. Science. 2001; 293:1159–1163. [PubMed: 11498596]
5. Buhl EH, Halasy K, Somogyi P. Diverse sources of hippocampal unitary inhibitory postsynaptic potentials and the number of synaptic release sites. Nature. 1994; 368:823–828. [PubMed: 8159242]
6. Pawelzik H, Hughes DI, Thomson AM. Physiological and morphological diversity of immunocytochemically defined parvalbumin- and cholecystokinin-positive interneurones in CA1 of the adult rat hippocampus. J. Comp. Neurol. 2002; 443:346–367. [PubMed: 11807843]
7. Lamsa KP, Heeroma JH, Somogyi P, Rusakov DA, Kullmann DM. Anti-Hebbian long-term potentiation in the hippocampal feedback inhibitory circuit. Science. 2007; 315:1262–1266. [PubMed: 17332410]

8. Fuchs EC, et al. Recruitment of parvalbumin-positive interneurons determines hippocampal function and associated behavior. Neuron. 2007; 53:591–604. [PubMed: 17296559]
9. Cossart R, et al. Interneurons targeting similar layers receive synaptic inputs with similar kinetics. Hippocampus. 2006; 16:408–420. [PubMed: 16435315]
10. Glickfeld LL, Scanziani M. Distinct timing in the activity of cannabinoid-sensitive and cannabinoid-insensitive basket cells. Nat. Neurosci. 2006; 9:807–815. [PubMed: 16648849]
11. Hajos N, et al. Spike timing of distinct types of GABAergic interneuron during hippocampal gamma oscillations in vitro. J. Neurosci. 2004; 24:9127–9137. [PubMed: 15483131]
12. Gloveli T, et al. Differential involvement of oriens/pyramidale interneurones in hippocampal network oscillations in vitro. J. Physiol. 2005; 562:131–147. [PubMed: 15486016]
13. Mann EO, Suckling JM, Hajos N, Greenfield SA, Paulsen O. Perisomatic feedback inhibition underlies cholinergically induced fast network oscillations in the rat hippocampus in vitro. Neuron. 2005; 45:105–117. [PubMed: 15629706]
14. Gulyás AI, et al. Parvalbumin-containing fast-spiking basket cells generate the field potential oscillations induced by cholinergic receptor activation in the hippocampus. J. Neurosci. 2010; 30:15134–15145. [PubMed: 21068319]
15. Klausberger T, et al. Brain-state- and cell-type-specific firing of hippocampal interneurons in vivo. Nature. 2003; 421:844–848. [PubMed: 12594513]
16. Gentet LJ, Avermann M, Matyas F, Staiger JF, Petersen CC. Membrane potential dynamics of GABAergic neurons in the barrel cortex of behaving mice. Neuron. 2010; 65:422–435. [PubMed: 20159454]
17. Gentet LJ, et al. Unique functional properties of somatostatin-expressing GABAergic neurons in mouse barrel cortex. Nat. Neurosci. 2012; 15:607–612. [PubMed: 22366760]
18. Csicsvari J, Hirase H, Czurko A, Mamiya A, Buzsaki G. Oscillatory coupling of hippocampal pyramidal cells and interneurons in the behaving Rat. J. Neurosci. 1999; 19:274–287. [PubMed: 9870957]
19. Maurer AP, Cowen SL, Burke SN, Barnes CA, McNaughton BL. Phase precession in hippocampal interneurons showing strong functional coupling to individual pyramidal cells. J. Neurosci. 2006; 26:13485–13492. [PubMed: 17192431]
20. Ego-Stengel V, Wilson MA. Spatial selectivity and theta phase precession in CA1 interneurons. Hippocampus. 2007; 17:161–174. [PubMed: 17183531]
21. Royer S, et al. Control of timing, rate and bursts of hippocampal place cells by dendritic and somatic inhibition. Nat. Neurosci. 2012; 15:769–775. [PubMed: 22446878]
22. Pinault D. A novel single-cell staining procedure performed in vivo under electrophysiological control: morpho-functional features of juxtacellularly labeled thalamic cells and other central neurons with biocytin or Neurobiotin. J. Neurosci. Methods. 1996; 65:113–136. [PubMed: 8740589]
23. Haiss F, Butovas S, Schwarz C. A miniaturized chronic microelectrode drive for awake behaving head restrained mice and rats. J. Neurosci. Methods. 2010; 187:67–72. [PubMed: 20036690]
24. Fazzari P, et al. Control of cortical GABA circuitry development by Nrg1 and ErbB4 signalling. Nature. 2010; 464:1376–1380. [PubMed: 20393464]
25. Fuentealba P, et al. Ivy cells: a population of nitric-oxide-producing, slow-spiking GABAergic neurons and their involvement in hippocampal network activity. Neuron. 2008; 57:917–929. [PubMed: 18367092]
26. Szabadics J, Soltesz I. Functional Specificity of Mossy Fiber Innervation of GABAergic Cells in the Hippocampus. J. Neurosci. 2009; 29:4239–4251. [PubMed: 19339618]
27. Tricoire L, et al. Common Origins of Hippocampal Ivy and Nitric Oxide Synthase Expressing Neurogliaform Cells. J. Neurosci. 2010; 30:2165–2176. [PubMed: 20147544]
28. Epsztein J, Brecht M, Lee AK. Intracellular determinants of hippocampal CA1 place and silent cell activity in a novel environment. Neuron. 2011; 70:109–120. [PubMed: 21482360]
29. Harvey CD, Collman F, Dombeck DA, Tank DW. Intracellular dynamics of hippocampal place cells during virtual navigation. Nature. 2009; 461:941–U196. [PubMed: 19829374]

30. O'Keefe J. Place units in the hippocampus of the freely moving rat. Exp. Neurol. 1976; 51:78–109. [PubMed: 1261644]
31. Olah S, et al. Regulation of cortical microcircuits by unitary GABA-mediated volume transmission. Nature. 2009; 461:1278–1281. [PubMed: 19865171]
32. Lubenov EV, Siapas AG. Hippocampal theta oscillations are travelling waves. Nature. 2009; 459:534–539. [PubMed: 19489117]
33. Hartwich K, Pollak T, Klausberger T. Distinct firing patterns of identified basket and dendrite-targeting interneurons in the prefrontal cortex during hippocampal theta and local spindle oscillations. J. Neurosci. 2009; 29:9563–9574. [PubMed: 19641119]
34. Klausberger T, Somogyi P. Neuronal diversity and temporal dynamics: the unity of hippocampal circuit operations. Science. 2008; 321:53–57. [PubMed: 18599766]
35. Ylinen A, et al. Sharp wave-associated high-frequency oscillation (200 Hz) in the intact hippocampus: network and intracellular mechanisms. J. Neurosci. 1995; 15:30–46. [PubMed: 7823136]
36. Vida I, Bartos M, Jonas P. Shunting inhibition improves robustness of gamma oscillations in hippocampal interneuron networks by homogenizing firing rates. Neuron. 2006; 49:107–117. [PubMed: 16387643]
37. Hu H, Martina M, Jonas P. Dendritic mechanisms underlying rapid synaptic activation of fast-spiking hippocampal interneurons. Science. 2010; 327:52–58. [PubMed: 19965717]
38. Losonczy A, Zemelman B, Vaziri A, Magee J. Network mechanisms of theta related neuronal activity in hippocampal CA1 pyramidal neurons. Nat. Neurosci. 2010; 13:967–972. [PubMed: 20639875]
39. Lovett-Barron M, et al. Regulation of neuronal input transformations by tunable dendritic inhibition. Nat. Neurosci. 2012; 15:423–430. [PubMed: 22246433]
40. Freund TF, Buzsaki G. Interneurons of the hippocampus. Hippocampus. 1996; 6:347–470. [PubMed: 8915675]
41. Foster DJ, Wilson MA. Reverse replay of behavioural sequences in hippocampal place cells during the awake state. Nature. 2006; 440:680–683. [PubMed: 16474382]
42. Diba K, Buzsaki G. Forward and reverse hippocampal place-cell sequences during ripples. Nat. Neurosci. 2007; 10:1241–1242. [PubMed: 17828259]
43. Markwardt SJ, Dieni CV, Wadiche JI, Overstreet-Wadiche L. Ivy/neurogliaform interneurons coordinate activity in the neurogenic niche. Nat. Neurosci. 2011; 14:1407–1409. [PubMed: 21983681]
44. Vizi ES. Role of high-affinity receptors and membrane transporters in nonsynaptic communication and drug action in the central nervous system. Pharm. Revs. 2000; 52:63–89. [PubMed: 10699155]
45. Lee AK, Manns ID, Sakmann B, Brecht M. Whole-cell recordings in freely moving rats. Neuron. 2006; 51:399–407. [PubMed: 16908406]
46. Hacker SO, White CE, Black IH. A comparison of target-controlled infusion versus volatile inhalant anesthesia for heart rate, respiratory rate, and recovery time in a rat model. Contemp. Top. Lab. Anim. Sci. 2005; 44:7–12. [PubMed: 16138774]
47. Lasztoczi B, Tukker JJ, Somogyi P, Klausberger T. Terminal Field and Firing Selectivity of Cholecystokinin-Expressing Interneurons in the Hippocampal CA3 Area. J. Neurosci. 2011; 31:18073–18093. [PubMed: 22159120]
48. Klausberger T, et al. Complementary roles of cholecystokinin- and parvalbumin-expressing GABAergic neurons in hippocampal network oscillations. J. Neurosci. 2005; 25:9782–9793. [PubMed: 16237182]
49. Louie K, Wilson MA. Temporally structured replay of awake hippocampal ensemble activity during rapid eye movement sleep. Neuron. 2001; 29:145–156. [PubMed: 11182087]
50. Berens P. CircStat: A MATLAB Toolbox for Circular Statistics. J.. Stat. Software. 2009; 31:1–21.

Europe PMC Funders Author Manuscripts

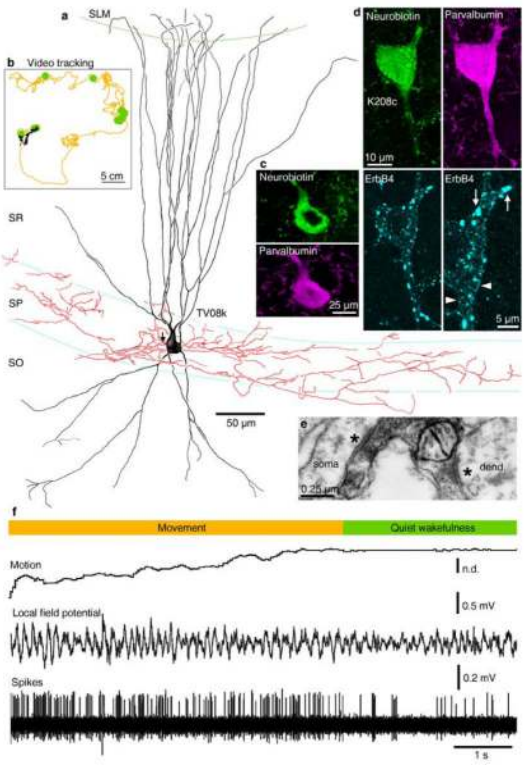

Figure 1. Firing patterns of an identified PV-expressing basket cell during different behavioral states

(a) Reconstruction of soma, dendrites (black, complete) and axon (red, one 70 µm thick-section). Arrow indicates the main axon. **(b)** Movements, quiet wakefulness (green circles) and those spikes occurring in the short trace in **f** (black dots) in the recording arena. **(c)** Confocal fluorescence images showing the cell body immunopositive for PV. **(d)** Immunopositive ErbB4 receptor-patches (arrows) and continuous membrane-labeling (arrowheads) of another recorded basket cell (K208c). **(e)** Electron-micrograph of an axonal bouton (from **a**) making type-II-synapses (asterisks) onto soma and dendrite of pyramidal cells. **(f)** The cell decreased firing at the transition between walking and quiet wakefulness. SLM, stratum-lacunosum-moleculare; SR, stratum-radiatum; SP, stratum-pyramidale; SO, stratum-oriens; n.d. normalized distance.

Europe PMC Funders Author Manuscripts

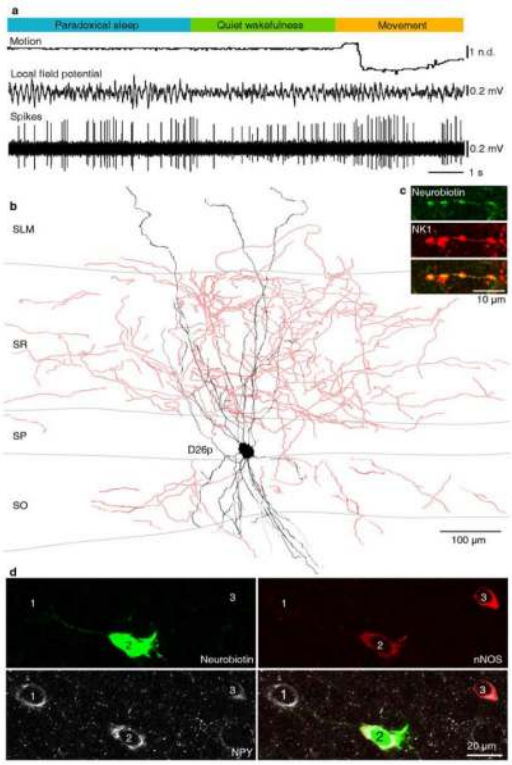

Figure 2. Firing patterns of an identified ivy cell during different behavioral states

(a) The cell fired with similar rates during paradoxical sleep, quiet wakefulness and body-movement. n.d., normalized distance. **(b)** Reconstruction of the cell (soma and dendrites black, complete; axon red, from one section of 70 µm thickness). **(c)** Confocal fluorescence images showing a dendrite of the cell immunopositive for the NK1 receptor. **(d)** The soma (2) is immunopositive for nNOS and NPY; note nearby unrecorded cells (1) immunopositive only for NPY, and a cell (3) positive for both NPY and nNOS.

Europe PMC Funders Author Manuscripts

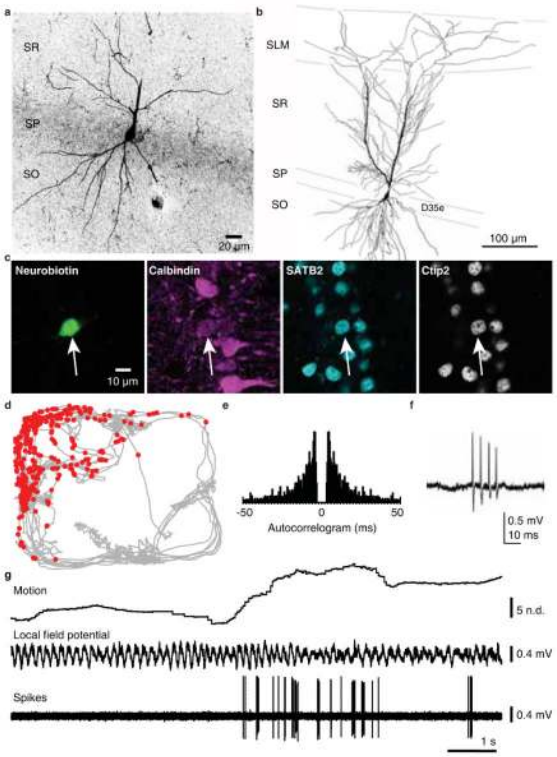

Figure 3. Molecular expression and firing patterns of a place cell

(a) The recorded pyramidal cell was labelled with neurobiotin and visualized by incubation with a streptavidin conjugated fluorophore (confocal z-stacks, projection of 10 optical sections around the soma) and **(b)** its full dendritic tree was reconstructed (6 sections of 70 µm thickness). **(c)** This cell is immunopositive for SATB2, Ctip2 and is weakly immunopositive for calbindin. **(d)** The superimposed spikes (filtered >5 cm/s; red dots) on the path (grey) of the animal indicate a spatial firing preference, the signature of a place cell. **(e)** Autocorrelogram of spike timing. **(f)** The cell discharged complex-spikes and **(g)** showed sparse firing and spatial related activity.

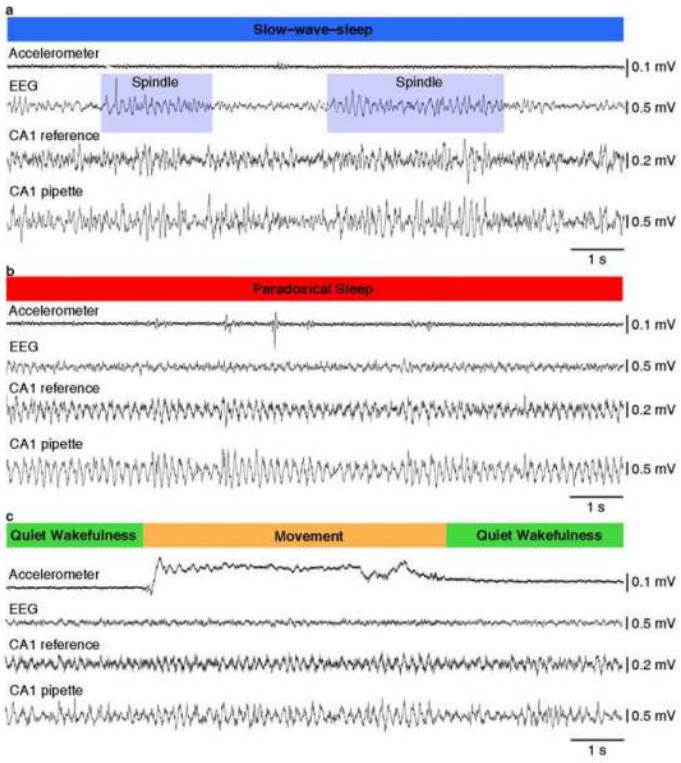

Figure 4. Behavioral state segmentation

(a) Slow-wave-sleep was characterized by EEG spindles (9-14Hz; purple rectangles) and large amplitude slow oscillations (< 3 Hz) associated with no movements detected on the accelerometer. **(b)** Predominant theta oscillations on all channels with an absence of movements, except for some fast twitches, defined paradoxical sleep episodes. **(c)** Wakefulness distinguished by a desynchronized low amplitude EEG was further segmented into quiet wakefulness and movement periods based on activity from the accelerometer.

Europe PMC Funders Author Manuscripts

Europe PMC Funders Author Manuscripts

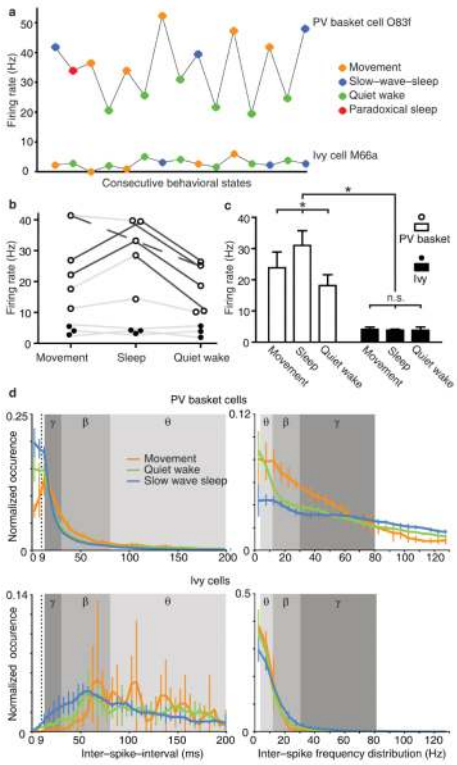

Figure 5. Differential firing of PV-expressing basket and ivy cells during distinct behavioral states

(a) Firing rates of a PV-expressing basket and an ivy cell during 15 consecutive behavioral states. **(b)** Individual PV-expressing basket cells (open circles) had different firing rates during movement, slow-wave-sleep (excluding paradoxical sleep) and quiet wakefulness, but none of the ivy cells (filled circles) changed firing rates. Lines connect data from individual cells, dark grey lines indicate $p<0.05$ for post-hoc Dunn tests after Kruskal Wallis test; dashed grey line indicates significant difference for a cell between movement and quiet wakefulness. **(c)** The mean firing rates of PV-expressing basket cells ($p=0.009$ for paired Friedman test; $p=0.004$ for repeated-measures ANOVA; $n=5$), but not ivy cells ($p=0.9$ for both paired Friedman test and repeated-measures ANOVA, $n=3$), differed during distinct behavioral states. A mixed-model two-way ANOVA analysis indicated significant differences between the factor cell type ($p=0.01$), the repeated-measure factor behavioral state ($p=0.005$) and the interaction of both factors ($p=0.03$) with a significant subject matching ($p<0.001$). Bars represent mean ± s.e.m.. **(d)** Inter-spike intervals and inter-spike frequency distributions differ between cell types and behavioral states. Data are shown as mean ± s.e.m. for PV-expressing basket ($n=5$) and ivy ($n=3$) cells. For each behavioral state of individual cells the occurrence was normalized so that the sum of all bins equals 1 for interspike intervals < 350 ms; note differences in scale between histograms.

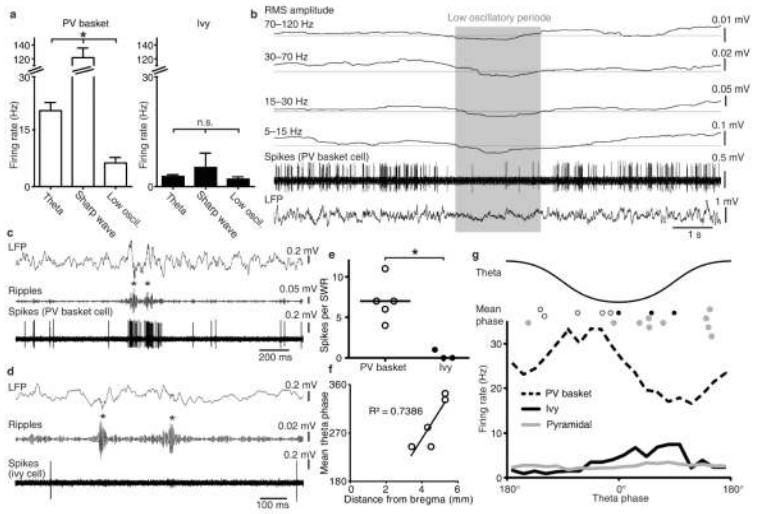

Figure 6. Differential firing of PV-expressing basket and ivy cells during network oscillations

(a) The mean firing rates of PV-expressing basket ($p=0.008$ for paired Friedman test; $p<0.0001$ for repeated-measure ANOVA; $n=5$) but not ivy ($p=0.4$ for paired Friedman test; $p=0.6$ for repeated-measure ANOVA; $n=3$) cells was different during theta oscillations, sharp wave-associated ripples and periods of low oscillatory activity (low oscil.) measured in the LFP. Bars represent mean ± s.e.m.. **(b)** Basket cell TV08k decreased firing during a period of low oscillatory activity, which was detected by a drop of the root-mean-square (RMS) amplitude below mean-SD (horizontal grey lines) simultaneous in four frequency bands of the LFP. **(c)** Basket cell D41n strongly increased firing but **(d)** ivy cell D26p was not activated during ripples (asterisks). **(e)** Different median number of spikes per sharp wave-associated ripple episode of PV-expressing basket ($n=5$) and ivy cells ($n=3$). **(f)** Mean firing phases of PV-expressing basket cells relative to the locally-detected theta oscillations was related to the position of the cells in the hippocampus. **(g)** Firing-phase-histograms for basket, ivy and pyramidal cells during theta oscillations. Mean firing phases of individual (circles) basket and ivy cells did not overlap.

Europe PMC Funders Author Manuscripts

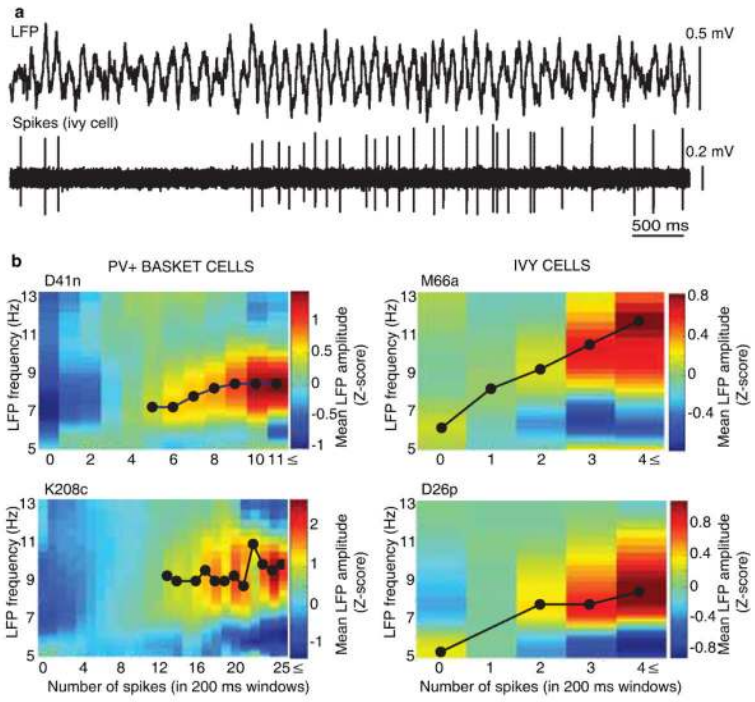

Figure 7. Relationship between frequency and amplitude of theta oscillations and the firing rate of PV-expressing basket and ivy cells

(a) Ivy cell D26p increases firing with higher frequency theta oscillations in the LFP. **(b)** Using a Morlet wavelet transformation the average amplitude (z-transformed, color-coded) and frequency of theta oscillations detected in the LFP are plotted as a function of instantaneous firing rate of individual cells (warmest and coldest colors correspond to maxima and minima over the whole plot). Note that the instantaneous rate is given as the number of spikes in a 200 ms window, so 0, 1 and 10 spikes correspond to 0 Hz, 5 Hz, and 50 Hz, respectively. Black circles indicate detected peaks in LFP amplitude.

Europe PMC Funders Author Manuscripts

Europe PMC Funders Author Manuscripts

Table 1

Neurochemical expression profile and firing patterns of recorded cells

cell group	cell	mean theta phase of firing	mean theta vector length of firing	median nb of spikes per ripple epsiode	Immunohistochemical test												
					parvalbumin	ErbB4	NPY	nNOS	NK1R	GABAARal	GABAAR6	CCK	reelin	somatostatir	SATB2	VIP	calbindin
PV basket cells	D41n	292.22	0.18	11	+ s	+ s	– s					– s					
	K208c	344.82	0.19	7	+ s,d	+ s,d				+ s,d		– s					
	LK08c	331.87	0.32	4	+ s,a	+ s	– s					nc		nc			
	O83f	232.77	0.2	7	+ s,d	+ s	– s							– s			
	TV08k	239.45	0.2	6	+ s,d	+ d	– s					nc		– s			
Ivy cells	B83k	86.63	0.62	0	– d		+ s	+ s	+ d	+ d	nc						
	D26p	50.22	0.45	0			+ s	+ s	+ d	+ d	+ d		– s			– d	
	ML66a	357.84	0.32	1	– d		+ s	– s	+ d	+ d	+ d						
Pyramidal cells	D19b	215.2	0.29	0													– d
	D30q	224.51	0.31	0													– d
	D35e	149.14	0.09	0								– d			+ s		+ s
	D36w	82.39	0.04	0													– d

"+" indicates immunopositive; "–" indicates that no specific immunoreactivity could be detected in this cell, although other immunopositive cells were observed nearby; "nc", not conclusive; "s", tested on soma; "d", tested on dendrite